

Cosmological models discrimination with Weak Lensing

Sandrine Pires¹, Jean-Luc Starck¹, Adam Amara^{1,2},
Alexandre Réfrégier¹, and Romain Teyssier¹

¹ Laboratoire AIM, CEA/DSM-CNRS-Universite Paris Diderot, IRFU/SEDI-SAP, Service d'Astrophysique, CEA Saclay, Orme des Merisiers, 91191 Gif-sur-Yvette, France

² Department of Physics, ETH Zürich, Wolfgang-Pauli-Strasse 16, CH-8093 Zürich, Switzerland

July 3, 2021

Abstract Weak gravitational lensing provides a unique method to map directly the dark matter in the Universe. The majority of lensing analyses uses the two-point statistics of the cosmic shear field to constrain the cosmological model yielding degeneracies, such as that between σ_8 and Ω_m , respectively the r.m.s. of the mass fluctuations at a scale of $8Mpc/h$ and the matter density parameter both at $z = 0$. However, the two-point statistics only measure the Gaussian properties of the field and the weak lensing field is non-Gaussian. It has been shown that the estimation of non-Gaussian statistics on weak lensing data can improve the constraints on cosmological parameters. In this paper, we systematically compare a wide range of non-Gaussian estimators in order to determine which one provides tighter constraints on the cosmological parameters. These statistical methods include skewness, kurtosis and the Higher Criticism test in several sparse representations such as wavelet and curvelet; as well as the bispectrum, peak counting and a new introduced statistic called Wavelet Peak Counting (*WPC*). Comparisons based on sparse representations show that the wavelet transform is the most sensitive to non-Gaussian cosmological structures. It appears also that the best statistic for non-Gaussian characterization in weak lensing mass maps is the *WPC*. Finally, we show that the σ_8 - Ω_m degeneracy could be even better broken if the *WPC* estimation is performed on weak lensing mass maps filtered by the wavelet method, MRLens.

Key words. Cosmology : Weak Lensing, Methods : Statistics, Data Analysis

1. Introduction

Images distortion measurements of background galaxies caused by large-scale structures provides a direct way to study the statistical properties of the growth of structures in the Universe. Weak gravitational lensing measures the mass and can thus be directly compared to theoretical models of structure formation. Most lensing studies use the two-point statistics of the cosmic shear field because

of its potential to constrain the power spectrum of density fluctuations in the late Universe (e.g. Maoli et al., 2001; Refregier et al., 2002; Bacon et al., 2003; Massey et al., 2005; Dahle, 2006). Two-point statistics measure the Gaussian properties of the field. This is a limited amount of information since it is well known that the low redshift Universe is highly non-Gaussian on small scales. Indeed, gravitational clustering is a non linear process and in particular at small scales the mass distribution is highly non-Gaussian. Consequently, using only two-point statistics to set constraints on the cosmological model is limited. Better constraints can be obtained using 3D weak lensing maps (Bernardeau et al., 1997; Pen et al., 2003;

Send offprint requests to: sandrine.pires@cea.fr

Massey et al., 2007). An alternative procedure is to consider higher-order statistics of the weak lensing shear field enabling a characterization of the non-Gaussian nature of the signal (see e.g. Takada and Jain, 2003; Jarvis et al., 2004; Kilbinger and Schneider, 2005; Hamana et al., 2004; Donoho and Jin, 2004).

In this paper, we systematically compare a range of non-Gaussian statistics. For this purpose, we focus on the degeneracy between σ_8 and Ω_m , respectively the amplitude of the matter power spectrum and the matter density parameter both at $z = 0$. We investigate which statistical method is the most efficient to break this degeneracy that exists when only the two-point correlation is considered. A wide range of statistical methods are systematically applied on a set of simulated data in order to characterize the non-Gaussianity present in the mass maps due to the growth of structures. Their performance to discriminate between different possible cosmological models are compared. For the CMB, it has been proposed to use statistics such wavelet kurtosis or wavelet Higher Criticism to detect clusters and curvelet kurtosis or curvelet Higher Criticism to detect anisotropic feature such cosmic strings (Jin et al., 2005). As weak lensing data may contain filamentary structures, we have also considered such statistical approaches based on sparse representations.

In section 2, we review the major statistical methods used in the literature to constrain cosmological parameters from weak lensing data. Section 3 describes the simulations used in this paper, especially how 2D weak lensing mass maps of five different models have been derived from large statistical samples of 3D N-body simulations of density distribution. Section 4 is dedicated to the description of our analysis and we introduce the different statistics we have studied along with the different multiscale transforms investigated. We also present a new statistic that we call Wavelet Peak Counting (WPC). In section 5, we present our results and finally, section 6 et section 7 present a discussion and summaries our conclusions.

2. Weak lensing statistics and cosmological models constraints: state of the art

2.1. Two-point statistics

The most common method for constraining cosmology in weak lensing studies uses two-point statistics of

the shear field calculated either in real or Fourier space. In general there is an advantage in using Fourier space statistics such as the power spectrum because the modes are independent. The power spectrum $P_\kappa(l)$ of the 2D convergence is defined as a function of the modes l by:

$$\langle \hat{\kappa}(\mathbf{l})\hat{\kappa}(\mathbf{l}') \rangle = (2\pi)^2 \delta(\mathbf{l} - \mathbf{l}') P_\kappa(l), \quad (1)$$

where hat symbols denotes Fourier transforms, δ is the delta function, the brackets denote an average over l . $P_\kappa(l)$ only depends on $l = |\mathbf{l}|$ and κ is the convergence (i.e. which is proportional to the projected mass distribution).

This power spectrum $P_\kappa(l)$ can be expressed in terms of the 3D matter power spectrum $P(k, \chi)$ of the mass fluctuations $\delta\rho/\rho$ and of cosmological parameters :

$$P_\kappa(l) = \frac{9}{16} \left(\frac{H_0}{c} \right)^2 (\Omega_m)^2 \int d\chi \left[\frac{g(\chi)}{ar(\chi)} \right]^2 P\left(\frac{l}{r}, \chi\right), \quad (2)$$

where a is the expansion parameter, H_0 is the Hubble constant and Ω_m is the matter density parameter. The correlation properties are more convenient in Fourier space, but for surveys with complicated geometry due to the removal of bright stars and artifacts, the missing data need proper handling (a review of the different existing methods can be found in Pires et al., 2008). Real space statistics are easier to estimate, but require more computational time. The following two-point statistics can be related to the underlying 3D matter power spectrum via the 2D convergence power spectrum $P_\kappa(l)$:

- The shear variance $\langle \gamma^2 \rangle$:

An example of real space two-point statistic is the shear variance, defined as the variance of the average shear $\bar{\gamma}$ evaluated in circular patches of varying radius θ_s . The shear variance $\langle \gamma^2 \rangle$ is related to the power spectrum $P_\kappa(l)$ of the 2D convergence by :

$$\langle \gamma^2 \rangle = \int \frac{dl}{2\pi} l P_\kappa(l) \frac{J_1^2(l\theta_s)}{(l\theta_s)^2}, \quad (3)$$

where J_n is a Bessel function of order n . This shear variance has been used in many weak lensing analysis to constrain cosmological parameters (Maoli et al., 2001; Hoekstra et al., 2006; Fu et al., 2008).

- The shear two-point correlation function :

The shear two-point correlation function is currently the most used statistic because it is easy to implement

and can be estimated even for complex geometry. It is defined as follow :

$$\xi_{i,j}(\theta) = \langle \gamma_i(\boldsymbol{\theta}') \gamma_j(\boldsymbol{\theta}' + \boldsymbol{\theta}) \rangle, \quad (4)$$

where $i, j = 1, 2$ and the averaging is done over pairs of galaxies separated by angle $\theta = |\boldsymbol{\theta}|$. By parity $\xi_{1,2} = \xi_{2,1} = 0$ and by isotropy $\xi_{1,1}$ and $\xi_{2,2}$ are functions only of θ . The shear two-point correlation functions can be related to the 2D convergence power spectrum by :

$$\xi_+(\theta) = \xi_{1,1}(\theta) + \xi_{2,2}(\theta) = \int_0^\infty \frac{dl}{2\pi} l P_\kappa(l) J_0(l\theta), \quad (5)$$

These two-point correlation functions are the most popular statistical tools and have been used in the most recent weak lensing analysis (Benjamin et al., 2007; Hoekstra et al., 2006; Fu et al., 2008).

- The variance of the aperture mass M_{ap} :

The aperture mass statistic has been introduced by Schneider et al. (1998). It defined a class of statistics referred to *aperture masses* associated with compensated filters. Several forms of filters have been suggested which trade locality in real space with locality in Fourier space. Considering the filter defined in Schneider (1996) with a cutoff at some scale θ_s . The variance of the aperture mass can be expressed as a function of the 2D convergence power spectrum by :

$$\langle M_{ap}^2(\theta_s) \rangle = \int \frac{dl}{2\pi} l P_\kappa(l) \frac{576 J_4^2(l\theta_s)}{(l\theta_s)^4}, \quad (6)$$

This statistic has been used in Van Waerbeke et al. (2002); Semboloni et al. (2006); Hoekstra et al. (2006); Fu et al. (2008).

Two-point cosmic shear measurements yield interesting constraints on the amplitude of the matter power spectrum σ_8 on which the lensing strongly depends. But, when deriving joint constraints, a degeneracy exists between σ_8 and Ω_m (see e.g. Maoli et al., 2001; Hoekstra et al., 2002; Semboloni et al., 2006). This degeneracy between σ_8 and Ω_m is typical of cosmic shear measurements using only two-point statistics.

Two-point statistics are insufficient to characterize non-Gaussian features. Non-Gaussianity produced by the non-linear evolution of the Universe is of great importance for the understanding of the physics of the Universe, and it may help to better discriminate the cosmological models.

2.2. Non-Gaussian statistics

In the standard structure formation model, initial random fluctuations are amplified by non-linear gravitational instability to produce a final distribution of mass which is highly non-Gaussian. The weak lensing field is thus highly non-Gaussian. On small scales, we can observe structures like galaxies and clusters of galaxies and on larger scales, we observe some filament structures. Detecting these non-Gaussian features in weak lensing mass maps can be very useful to constrain the cosmological model parameters.

The three-point correlation function $\xi_{i,j,k}$ is the lowest-order statistics which can be used to detect non-Gaussianity.

$$\xi_{i,j,k}(\boldsymbol{\theta}) = \langle \kappa(\boldsymbol{\theta}_1) \kappa(\boldsymbol{\theta}_2) \kappa(\boldsymbol{\theta}_3) \rangle, \quad (7)$$

In Fourier space it is called bispectrum and only depends on distances $|\mathbf{l}_1|$, $|\mathbf{l}_2|$ and $|\mathbf{l}_3|$:

$$B(|\mathbf{l}_1|, |\mathbf{l}_2|, |\mathbf{l}_3|) \propto \langle \hat{\kappa}(|\mathbf{l}_1|) \hat{\kappa}(|\mathbf{l}_2|) \hat{\kappa}^*(|\mathbf{l}_3|) \rangle. \quad (8)$$

It has been shown that tighter constraints can be obtained with the three-point correlation function (Bernardeau et al., 1997; Cooray and Hu, 2001; Bernardeau et al., 2003; Takada and Jain, 2003, 2004; Schneider and Lombardi, 2003; Schneider et al., 2005; Benabed and Scoccimarro, 2006).

A simpler quantity than the three-point correlation function is provided by measuring the third-order moment (skewness) of the smoothed convergence κ (Bernardeau et al., 1997) or of the aperture mass M_{ap} (Jarvis et al., 2004; Kilbinger and Schneider, 2005).

Another approach to look for non-Gaussianity is to perform a statistical analysis directly on non-Gaussian structures like clusters. Galaxy clusters are the largest virialized cosmological structures in the Universe. They provide a unique way to focus on non-Gaussianity present at small scales. One interesting statistic is the *peak counting* that searches the number of peaks detected on the 2D convergence corresponding to the cluster abundance (see e.g. Hamana et al., 2004).

The methods to search for non-Gaussianity in the weak lensing literature mainly concentrate on higher-order correlation function. For the CMB, skewness and kurtosis of the wavelet coefficients are standard tools as well to check the CMB Gaussianity (Vielva et al., 2004; Starck et al., 2006; Vielva et al., 2006; Wiaux et al., 2008), and it was shown that curvelets (Starck et al.,

2003) were useful for the detection of anisotropic feature such cosmic string in the CMB (Starck et al., 2004; Jin et al., 2005).

In this following, we perform a comparison between most existing methods in order to find the best higher order statistic to constrain cosmological parameters from weak lensing data. To explore the effectiveness of a non-Gaussian measure we use a battery of N-Body simulations. By choosing five models whose two-point correlation statistics are degenerate, we study which statistics are able to distinguish between these models.

3. Simulations of weak lensing mass maps

3.1. 3D N-body cosmological simulations

We have run realistic simulated convergence mass maps derived from N-body cosmological simulations using the RAMSES code (Teyssier, 2002). The cosmological models are taken to be in concordance with the Λ CDM model. We have limited the model parameters to a realistic range (see Table 1) choosing five models along the (σ_8, Ω_m) -degeneracy discussed in §2.1.

Model	Box	Ω_m	Ω_L	h	σ_8
model 1	165.8	0.23	0.77	0.594	1
model 2	159.5	0.3	0.7	0.7	0.9
model 3	152.8	0.36	0.64	0.798	0.8
model 4	145.7	0.47	0.53	0.894	0.7
model 5	137.5	0.64	0.36	0.982	0.6

Table 1. Parameters of the five cosmological models that have been chosen along the (σ_8, Ω_m) -degeneracy. The box side is in Mpc/h, the simulations have 256^3 particles, Ω_m is the matter density parameter, Ω_L is the dark energy density parameter, h is equal to $H_0/100$ where H_0 is the Hubble constant and σ_8 the amplitude of the matter power spectrum.

For each of our five models, we run 21 N-Body simulations, each containing 256^3 particles. We refined the base grid of 256^3 cells when the local particle number exceeds 10. We further refined similarly each additional levels up to a maximum level of refinement of 6, corresponding to a spatial resolution of 10 kpc.h^{-1} .

3.2. 2D Weak lensing mass map

In N-body simulations, which are commonly used in cosmology, the dark matter distribution is represented using discrete massive particles. The simplest way to treat these particles is to map their positions onto a pixelised grid. In the case of multiple sheet weak lensing, we do this by taking slices through the 3D simulations. These slices are then projected into 2D mass sheets.

The effective convergence can subsequently be calculated by stacking a set of these 2D mass sheets along the line of sight, using the lensing efficiency function. This is a procedure that has been used before by Vale and White (2003), where the effective 2D mass distribution κ_e is calculated by integrating the density fluctuation along the line of sight. Using the Born approximation which neglects the facts that the light rays don't follow straight lines, the convergence can be numerically expressed by :

$$\kappa_e \approx \frac{3H_0^2 \Omega_m L}{2c^2} \sum_i \frac{\chi_i(\chi_0 - \chi_i)}{\chi_0 a(\chi_i)} \left(\frac{n_p R^2}{N_t s^2} - \Delta r_{f_i} \right), \quad (9)$$

where H_0 is the Hubble constant, Ω_m is the density of matter, c is the speed of light, L is the length of the box, χ are co-moving distances, with χ_0 being the co-moving distance to the source galaxies. The summation is performed over the i^{th} box. The number of particles associated with a pixel of the simulation is n_p , the total number of particles within a simulation is N_t and $s = L_p/L$ where L_p is the length of the plane doing the lensing. R is the size of the 2D maps and $\Delta r_{f_i} = \frac{r_2 - r_1}{L}$ where r_1 and r_2 are co-moving distances.

Using the previous 3D N-body simulations, we have derived 100 realizations for the five models. Fig. 1 shows one realization of the convergence for each of the 5 models. In all cases, the field is $3.95^\circ \times 3.95^\circ$, downsampled to 1024^2 pixels and we assume that the sources lie at exactly $z = 1$. At large scale, the map shows clearly a Gaussian signal. On the contrary, at small scales, the signal is clearly dominated by clumpy structures (dark matter halos) and is therefore highly non-Gaussian.

3.3. 2D Weak lensing noisy mass map

In practice, the observed shear γ_i is obtained by averaging over a finite number of galaxies and is therefore noisy. The noise arises both from the measurement errors and from the intrinsic ellipticities dispersion of galaxies.

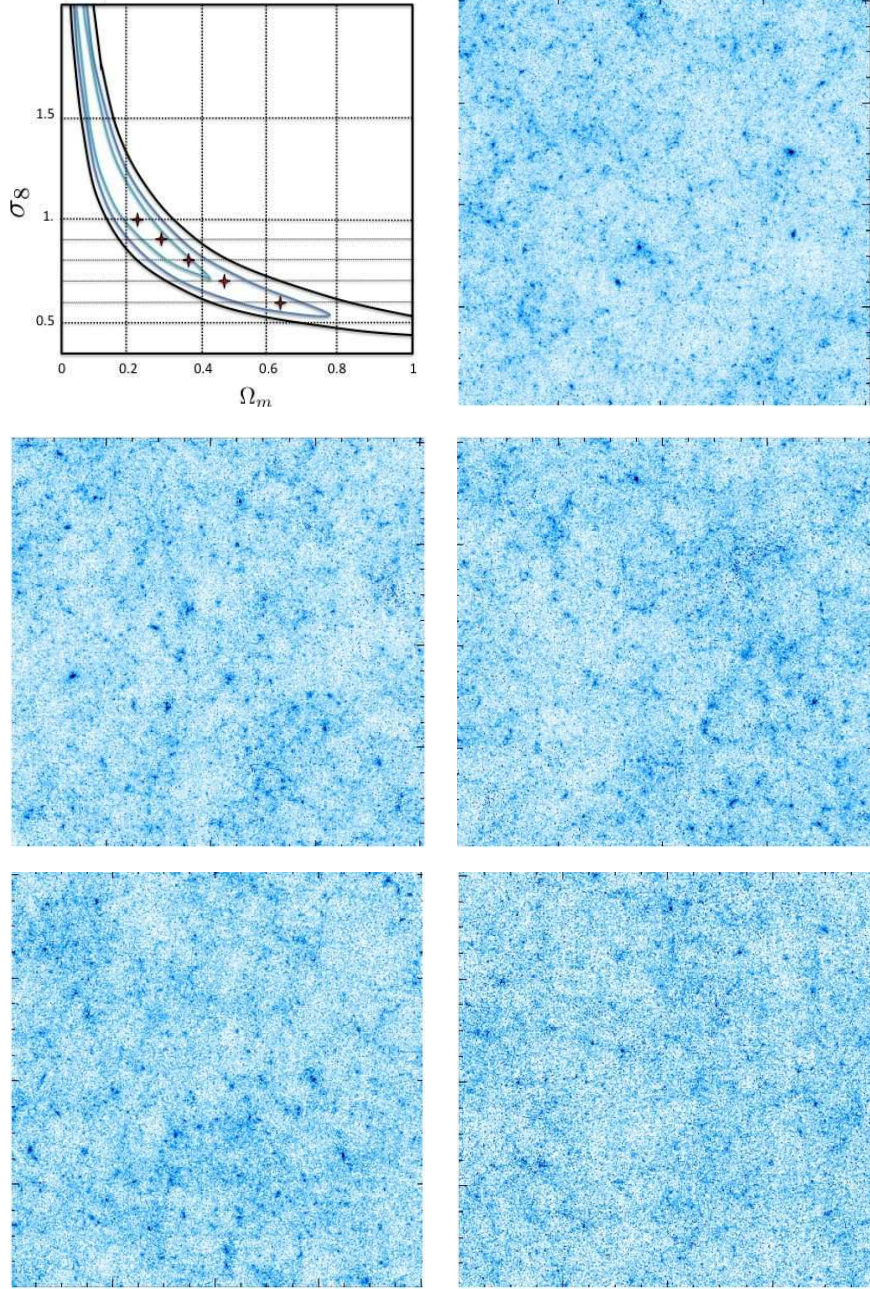


Figure 1. Upper left, the 5 cosmological models along the (σ_8, Ω_m) -degeneracy. Upper right, one realization of the convergence κ for model 1 ($\sigma_8 = 1$ and $\Omega_m = 0.23$); middle left, for model 2 ($\sigma_8 = 0.9$ and $\Omega_m = 0.3$); middle right, for model 3 ($\sigma_8 = 0.8$ and $\Omega_m = 0.36$); bottom left, for model 4 ($\sigma_8 = 0.7$ and $\Omega_m = 0.47$) and bottom right for model 5 ($\sigma_8 = 0.6$ and $\Omega_m = 0.64$). Each map is 1.975×1.975 degrees down-sampled to 512×512 pixels

As a good approximation, we modeled the noise as an uncorrelated Gaussian random field with variance :

$$\sigma_{noise}^2 = \frac{\sigma_\epsilon^2}{A.n_g}, \quad (10)$$

where A is the pixel size in arcmin^2 , n_g the average number of galaxies per arcmin^2 and σ_ϵ the rms of the shear distribution. We assume $\sigma_\epsilon \simeq 0.3$ per shear component and $n_g = 100 \text{ gal/arcmin}^2$ as is approximately found for space-based weak lensing surveys (Massey et al., 2004). An estimate of the noisy convergence κ_n is obtained using the least square estimator defined in Starck et al. (2006).

4. Cosmological model discrimination framework

In this study, in order to find the best statistic to break the (σ_8, Ω_m) -degeneracy, we are interested in comparing different statistics estimated in different representations using the set of simulated data described in the previous section.

For this purpose, for each statistic, we need to characterize, the discrimination obtained between each couple of models. The best statistic will be the one that maximizes the discrimination for all the couples of models.

4.1. Characterization of the discrimination

To find the best statistic, we need to characterize quantitatively for each statistic the discrimination between two different models m_1 and m_2 . One way to proceed is to define a discrimination efficiency that expresses the ability of a statistic to discriminate in percentage. Then, we need to define for each individual statistic, two different thresholds (see Fig. 2):

- a threshold \mathcal{T}_1 : if the estimation of a given statistic in a map κ_i is below \mathcal{T}_1 the map κ_i is classified belonging to the model m_1 and not if it is above
- a threshold \mathcal{T}_2 : if the estimation of a given statistic in a map κ_i is above \mathcal{T}_2 the map κ_i is classified belonging to the model m_2 and not if it is below. We have used a statistical tool called FDR (False Discovery Rate) introduced by Benjamini and Hochberg (1995) to set these two thresholds (\mathcal{T}_1 and \mathcal{T}_2) correctly (see Appendix A).

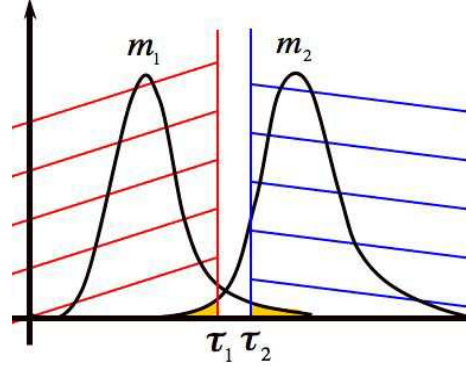


Figure 2. The following two distributions correspond to the histogram of the values of a given statistic estimated on the 100 realizations of model 1 (m_1) and on the 100 realizations of model 2 (m_2). The discrimination achieved with this statistic between m_1 and m_2 is rather good : the two distributions barely overlap. To characterize more quantitatively the discrimination, the FDR method has been used to estimate the thresholds \mathcal{T}_1 and \mathcal{T}_2 . A false discovery rate (α) equal to 0.05 has been chosen. Then a discrimination efficiency can be derived.

This FDR method is a competitive tool to set a threshold in an adaptive way without any assumption, given a false discovery rate (α). The false discovery rate is given by the proportion of false detections over the total number of detections. The threshold being estimated, we can derive a discrimination efficiency for each statistic. The discrimination efficiency measures the ability of a statistic to discriminate a model from another one by calculating the percentage of detections (true or false) over the total number of samples. It corresponds basically to the part of the distribution that doesn't overlap. The more the distributions overlap, the lower the discrimination efficiency will be.

The Fig. 2 represents the dispersion of the values of a given statistic estimated on the 100 realizations of the model 1 (on the left) and on the 100 realizations of the model 2 (on the right). The two distributions barely overlap, it indicates a good discrimination that is to say the two models can

easily be separated with this statistic. To be more quantitative, a threshold has been set for each distribution to estimate a discrimination efficiency that corresponds to the part of the distribution delimited by the hatched area.

The formalism of the FDR method ensures that the yellow area delimited by \mathcal{T}_1 (resp. \mathcal{T}_2) that corresponds to the false detections will be small.

4.2. A set of statistical tools

The first objective of this study is to compare different statistics to find the one that sets tighter constraints on the cosmological parameters. The two-point statistics that contain all the information about Gaussian signal leading to the (σ_8, Ω_m) -degeneracy, we have opted for statistics currently used to detect non-Gaussianity in order to probe the non-linear process of gravitational clustering. The statistics that we have selected are the following :

- Skewness (S_κ):
The skewness is the third-order moment of the convergence κ and is a measure of the asymmetry of a distribution. The convergence skewness is primarily due to rare and massive dark matter halos. The distribution will be more or less skewed positively depending on the abundance of rare and massive halos.
- Kurtosis (K_κ):
The kurtosis is the fourth-order moment of the convergence κ and is a measure of the peakedness of a distribution. A high kurtosis distribution has a sharper "peak" and flatter "tails", while a low kurtosis distribution has a more rounded peak with wider "shoulders".
- Bispectrum (B_κ):
Recently, there has been a lot of theoretical works on the three-point correlation function to constrain the cosmological parameters. But the direct computation of three-point correlation function takes too long for our large maps. We have then used its Fourier analog: the Bispectrum that has been introduced §2.2. And we have consider the equilateral configuration.
- Higher Criticism (HC):
HC is a recently developed statistic, proposed by Donoho and Jin (2004). It is a measure of non-Gaussianity obtained by looking at the maximum deviation comparing the sorted p -values of a distribution with the sorted p -values of a normal distribution. A

large HC value implies non-Gaussianity. We consider the two different forms of HC (see Appendix B) :

- HC*
- HC+
- Peak counting (P_c):
We now investigate the possibility of using the peak counting to differentiate among cosmological models. By peak counting (or cluster count), we mean the number of halos that we can detect per unit area of the sky (identified as peak above a mass threshold in mass maps). This cluster count enables to constrain the matter power spectrum normalization σ_8 for a given Ω_m (see e.g. Bahcall and Fan, 1998) and the formalism exist to predict the peak count to a given cosmological model (see e.g. Hamana et al., 2004).
- Wavelet Peak Counting (WPC):
We introduce a new statistic that we call Wavelet Peak Counting (WPC). This statistic consists in estimating a cluster count per scale of a wavelet transform. It means we have roughly a cluster count depending on the size of the clusters. We show in the following that the WPC is better than the peak counting to characterize the non-linear structure formation process.

All the statistics are estimated on the 2D convergence κ map. In practice the complex geometry of surveys gives the convergence κ inferred from the shear field γ_i the same complex geometry. But it becomes possible with the inpainting method developed in Pires et al. (2008) to reconstruct a full convergence κ map. The solution that is proposed enables to fill-in judiciously masked regions so as to reduce the impact of missing data on the estimation of the power spectrum and of higher-order statistical measures while requiring $O(N \log N)$ operations.

4.3. Representations

The second objective of the present study is to compare different transforms to find the sparsest representation of weak lensing data that makes the discrimination easier. Some studies on CMB data have used multiscale methods to detect non-Gaussianity (Aghanim and Forni, 1999; Starck et al., 2004). Weak lensing maps exhibit both isotropic and anisotropic features. These kind of features can be better represented in some basis functions. Indeed, a transform is optimal to detect structures which have the same shape of its basis elements. We have thus tested different representations :

- The Fourier transform
- The anisotropic bi-orthogonal wavelet transform
We expect the bi-orthogonal wavelet transform to be optimal for detecting mildly anisotropic features.
- The isotropic "à trous" wavelet transform
This wavelet transform is well adapted to the detection of isotropic features such as the clumpy structures (clusters) of the weak lensing data.
- The ridgelet transform
The ridgelet transform has been developed to process images including ridge elements, and so provides a good representation of perfectly straight edges.
- The curvelet transform
The curvelet transform allows to approximate curved singularities with few coefficients and then provides a good representation of curved structures.

A description of these transforms is available in Appendix C. We have to notice that the estimation of a given statistic at each resolution level of a representation can be considered as an individual statistic by itself.

5. Analysis and results

5.1. Treatment of the noise

As explained previously, the weak lensing mass maps are measured from the distortions of a finite number of background galaxies and therefore suffer from shot noise. Furthermore each galaxy provides only a noisy estimator of the distortion field. We have added the expected level of Gaussian noise (see §3.3) to simulations of weak lensing mass maps to obtain simulated noisy mass maps corresponding to space observations. Fig. 3 shows a noiseless simulated mass map (left) and a noisy simulated mass map (right) corresponding to space observations.

The noise has an impact on the estimated statistics and therefore needs to be considered.

5.1.1. No filtering

We begin by applying the different transformations directly to the noisy data and for each representation, we have estimated the statistics described in the previous section, with the exception of cluster count and *WPC* which required filtering.

We expect that the noise will make the third and fourth order statistics tend to zero. Indeed the more noisy

the data are, the more the distribution will look like a Gaussian.

5.1.2. Gaussian filtering

As a second step, we have performed a Gaussian filtering that is obtained by convolving the noisy mass maps κ_n with a Gaussian window G with a standard deviation σ_G :

$$\kappa_G = G * \kappa_n. \quad (11)$$

Fig. 4 shows on the left, the original map without noise and on the right, the result obtained by Gaussian filtering of the noisy mass map displayed in Fig. 3 (right). The quality of the filtering depends strongly on the value of σ_G . For the simulations, an optimal value is about 0.9 arcmin). We then computed all our statistics on this new set of filtered mass maps.

5.1.3. MRLens filtering

Finally, we used a method of non-linear filtering based on the wavelet representation : the MRLens filtering proposed by Starck et al. (2006). **The MRLens filtering is based on the Bayesian ideas that provides the means to incorporate prior knowledge in data analysis. Choosing the prior is one of the most critical aspects of Bayesian analysis. Here a multiscale entropy prior is used. A full description of the method is given in the Appendix D. The MRLens software that we used is available at the following address : <http://www-irfu.cea.fr/Ast/878.html>.**

It was shown in Starck et al. (2006) that this method outperforms several standard techniques (Gaussian filtering, Wiener filtering, MEM filtering, etc.). Fig. 5 shows on the left, the original map without noise and on the right, the result of a FDR filtering on the noisy mass map displayed Fig. 3 (right). The visual aspect indicates that many clusters are reconstructed and the intensity of the peaks are well recovered.

As done before, all the statistics have been estimated on these MRLens filtered mass maps. By reconstructing essentially the clusters, we can anticipate that this MRLens method will help statistics like peak counting or WPC more than statistics that focus on the background.

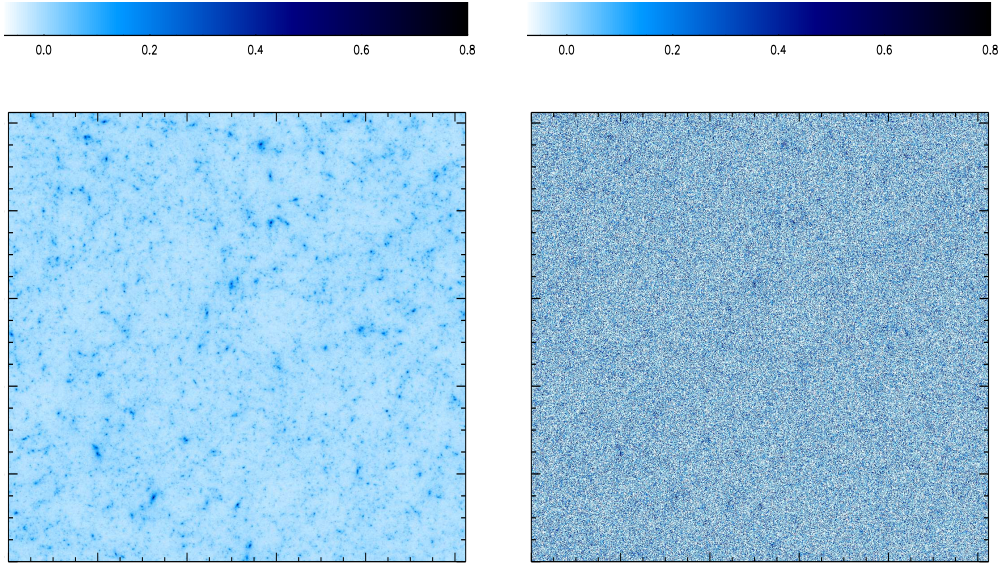


Figure 3. Left: noiseless simulated mass map and right: simulated noisy mass map that we should obtain in space observations. The field is $1.975^\circ \times 1.975^\circ$.

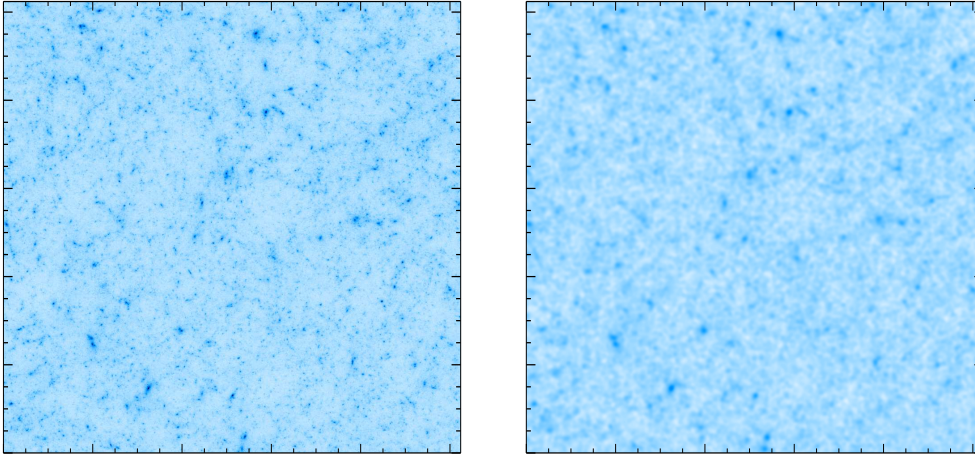


Figure 4. Left, noiseless simulated mass map, and right, filtered mass map by convolution with a Gaussian kernel. The field is $1.975^\circ \times 1.975^\circ$.

5.2. Results

5.2.1. The discrimination methodology

As explained section 4.1, for each statistic described in the previous section, we can derive a discrimination efficiency between each two mod-

els out of the full set of 5 models. This values are given Table 3, Table 5 and Table 7 for three different statistics.

A mean discrimination efficiency for each individual statistic can be estimated by averaging the discrimination efficiency across all the pairs of models. For statistics estimated in multiscale rep-

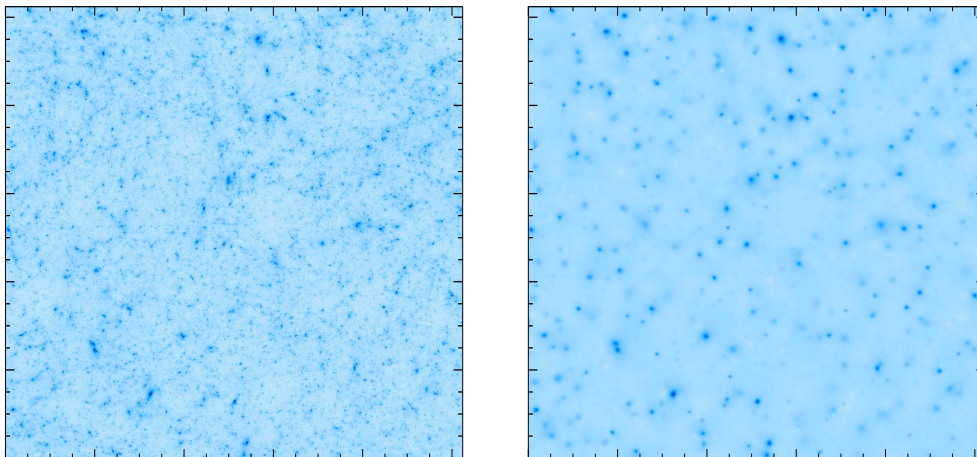


Figure 5. Left, noiseless simulated mass map, and right, filtered mass map by the FDR multiscale entropy filtering. The field is $1.975^\circ \times 1.975^\circ$.

representations, the mean discrimination efficiency is calculated for each scale and it is the better one that is considered.

Tables 2, 4 and 6 show the mean discrimination efficiency reached by a given statistic and a given transform, respectively for (i) unfiltered mass maps, (ii) Gaussian filtered mass maps and (iii) MRLens mass maps.

The mean discrimination efficiency of the Table 3 is about 40% and corresponds to the value at position (1,3) of Table 2 (i.e. the skewness of wavelet coefficients). And, the mean discrimination efficiency of Table 7 is about 97% and corresponds to the value at position (3,5) of Table 6.

A full discrimination between the five models is obtained if the mean discrimination efficiency is about 100%. If it is between 80% and 100% the discrimination is possible except for adjacent models. Less than 40% there is no discrimination possible even for distant models.

5.2.2. Discrimination in noisy mass maps

The mean discrimination efficiency obtained for unfiltered mass maps is displayed in Table 2. The peak counting and WPC differ from the others. They can not be computed on unfiltered mass maps because the clusters can not be extracted from noisy mass maps. Another point

is that the bispectrum by definition can only be estimated in the Fourier domain.

Without filtering the results are poor and no discrimination can be achieved in Direct space. Indeed, the Signal-to-Noise Ratio is weak as can be seen in Fig. 3 (right). The non-Gaussian signal is hidden by the Gaussian noise.

The different transforms appear to be inefficient at bring out the non-Gaussianity features, except, the Isotropic Wavelet Transform (see Table 2) which performs rather well, whatever the statistic. This is likely because it is optimal to detect clusters. Indeed, the clusters are a direct probe of non-Gaussianity and by concentrating the cluster information, the isotropic wavelet transform seems to be a better representation for non-Gaussianity.

The skewness in the Wavelet transform representation appears to be the best statistic in unfiltered mass maps. Table 3 shows the discrimination efficiency obtained with the skewness at the second scale of an Isotropic Wavelet Transform being the scale that reaches the best discrimination. We can see that the discrimination is only achieved between the farthest models, which is quite poor. **It is illustrated on Fig. 6 where you can see that the 5 distributions are overlapping.** Some groups have already used the skewness aperture mass statistic to try to break the σ_8 - Ω_m degeneracy, (see e.g. Kilbinger and Schneider, 2005; Jarvis et al., 2004). This processing consists of convolving the noisy signal by Gaussian windows with different scales and is quite simi-

Basis/Statistics	S	K	HC_n^*	HC_n^+	B_l	P_c	WPC
Direct space	21.0	1.6	1.8	1.9	x	x	x
Fourier space	0.7	10.7	3.0	21.3	5.75	x	x
Isotropic Wavelet Transform	40.5	29.3	24.9	34.0	x	x	x
Bi-orthogonal Wavelet Transform	7.3	10.8	4.1	2.9	x	x	x
Ridgelet Transform (block = 16)	6.2	3.7	7.2	5.6	x	x	x
Ridgelet Transform (block = 32)	8.3	15.2	9.5	20.4	x	x	x
Fast Curvelet Transform	1.1	4.2	2.6	4.2	x	x	x

Table 2. Mean discrimination efficiencies (in percent) achieved on noisy mass maps with a False Discovery Rate $\alpha = 0.05$.

lar to an Isotropic Wavelet Transform. They showed that by combining the second and third-order statistics, the degeneracy can be diminished but not broken.

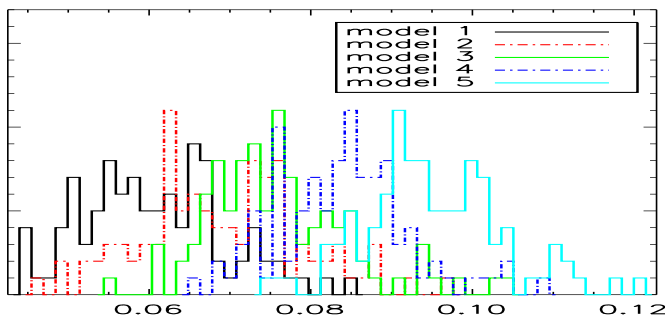


Figure 6. Distribution of the skewness calculated from the second scale of an Isotropic Wavelet Transform on the simulated realizations of the 5 models. It illustrates the results of the Table 3. No discrimination is possible except between the farthest models (i.e. between model 1 and model 5)

5.2.3. Discrimination in Gaussian filtered mass maps

To increase the Signal-to-Noise Ratio, we have applied a Gaussian filtering to the noisy simulated mass maps. Table 4 shows the results.

After Gaussian filtering, the noise is removed but the structures are over-smoothed. Except for the direct space where the results are clearly improved by the noise removal, the results after a Gaussian filtering are quite sim-

ilar. Some statistics are a bit improved by the noise removal while others become worse.

By contrast, the peak counting and WPC that can now be estimated on these filtered mass maps perform well. Table 5 shows the discrimination efficiency obtained with peak counting estimated on Gaussian filtered mass maps. We can see that except for adjacent models, discrimination is now possible. **We can verify this results by looking at the 5 distributions displayed Fig. 7. Indeed, the distributions barely overlap for no adjacent models.**

The ability of weak lensing cluster count (peak counting) to discriminate between the five different models chosen along the degeneracy can be explained. Considering that the dark matter lies at $z \simeq 0.5$, which is the maximum lensing efficiency for background galaxies at $z = 1$, and assuming a constant dark energy model, the number density of massive clusters in the weak lensing mass maps is sensitive to both the amplitude of the mass fluctuations σ_8 and the matter density parameter Ω_m , both at $z = 0$. If instead of σ_8 , we consider $\sigma_8^{z \simeq 0.5}$ that corresponds to the amplitude of the fluctuations of the projected weak lensing mass map. The $\sigma_8^{z \simeq 0.5}$ is now a constant along the five models because the five corresponding weak lensing power spectrum are undistinguishable. This leaves the Ω_m parameter that drives the structure formation (see e.g. Bahcall and Fan, 1998). A small Ω_m makes the structures form earlier and a large Ω_m makes the structures form later. Then, with a small Ω_m , the abundance of massive clusters at $z \simeq 0.5$ are more significant (see Fig. 1 upper right) than for a large Ω_m . The cluster count can then be used to discriminate cosmological model. The massive cluster abundance has already been used to probe Ω_m (see e.g. Bahcall and Fan, 1998).

	model 1	model 2	model 3	model 4	model 5
model 1	x	4	55	86	99
model 2	6	x	8	52	88
model 3	23	3	x	6	77
model 4	81	7	2	x	13
model 5	99	81	12	9	x

Table 3. Discrimination efficiencies (in percent) achieved on unfiltered mass maps with the skewness estimated at the second scale of an Isotropic Wavelet Transform.

Basis/Statistics	S	K	HC_n^*	HC_n^+	B_l	P_c	WPC
Direct space	39.2	34.3	28.8	40.2	x	79.3	x
Fourier space	2.2	2.2	3.8	2.9	6.75	x	x
Isotropic Wavelet Transform	31.9	29.5	24.	38.4	x	x	79.2
Bi-orthogonal Wavelet Transform	12.2	10.5	5.1	6.8	x	x	x
Ridgelet Transform (block = 16)	7.4	20.2	22.7	35.3	x	x	x
Ridgelet Transform (block = 32)	2.5	7.3	4.	9.1	x	x	x
Fast Curvelet Transform	1.3	4.7	4.8	8.3	x	x	x

Table 4. Mean discrimination efficiencies (in percent) achieved on Gaussian filtered mass maps with a False Discovery Rate $\alpha = 0.05$.

	model 1	model 2	model 3	model 4	model 5
model 1	x	50	95	100	100
model 2	46	x	43	96	100
model 3	94	8.	x	63.	100
model 4	100	97	50	x	78
model 5	100	100	99	63	x

Table 5. Discrimination efficiencies (in percent) achieved on Gaussian filtered mass maps with the peak counting statistic on direct space given a False Discovery Rate $\alpha = 0.05$.

5.2.4. Discrimination in MRLens filtered mass maps

Table 6 shows the results obtained in the case where the MRLens filtering scheme is applied to the noisy simulated mass maps.

After MRLens filtering, the sensitivity of all transforms is greatly improved. But, the Isotropic Wavelet Transform remains the best transform certainly helped by the MRLens filtering that uses this transform.

The best statistics remains the peak counting, which is also helped by the MRLens filtering that reconstructs essentially the clusters. But the others statistics also achieve quite good results in these MRLens filtered mass maps compared with the one with Gaussian filtered mass

maps. This is likely because the MRLens filtering by favoring the clusters reconstruction helps all the statistics that look for non-Gaussianity.

The best result is obtained with WPC on the third scale of the Isotropic wavelet transform see Table 7. **Fig. 8 shows the 5 distributions that barely overlap.** This statistic allows us to discriminate between different models even for adjacent models for which the discrimination is challenging.

The comparison of these results with the results obtained on noisy mass maps by the skewness in a wavelet representation (Table 3) show that the accuracy on σ_8 and

Basis/Statistics	S	K	HC_n^*	HC_n^+	B_l	P_c	WPC
Direct space	65.2	54.5	72.9	8.4	x	93.2	x
Fourier space	3.2	3.4	30.0	38.4	9.95	x	x
Isotropic Wavelet Transform	81.7	68.1	74.8	74.1	x	x	97.3
Bi-orthogonal Wavelet Transform	52.2	67.3	29.7	65.0	x	x	x
Ridgelet Transform (block = 16)	45.1	54.5	77.1	37.2	x	x	x
Ridgelet Transform (block = 32)	61.5	52.6	70.3	69.0	x	x	x
Fast Curvelet Transform	25.	65.5	68.8	63.3	x	x	x

Table 6. Mean discrimination efficiencies (in percent) achieved on MRLens filtered mass maps with a False Discovery Rate $\alpha = 0.05$.

	model 1	model 2	model 3	model 4	model 5
model 1	x	86	100	100	100
model 2	87	x	94	100	100
model 3	100	92	x	94	100
model 4	100	100	93	x	99
model 5	100	100	100	100	x

Table 7. Discrimination efficiencies (in percent) achieved on MRLens filtered mass maps with WPC at the third scale of an Isotropic Wavelet Transform.

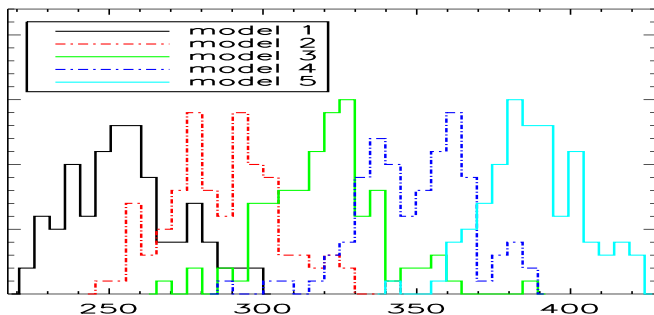


Figure 7. Distribution of the peak counting estimated directly on the simulated realizations of the 5 models. It illustrates the results of the Table 5. The discrimination is possible except between adjacent models (that is to say between model 1 and model 2, model 2 and model 3, model 3 and model 4, model 4 and model 5).

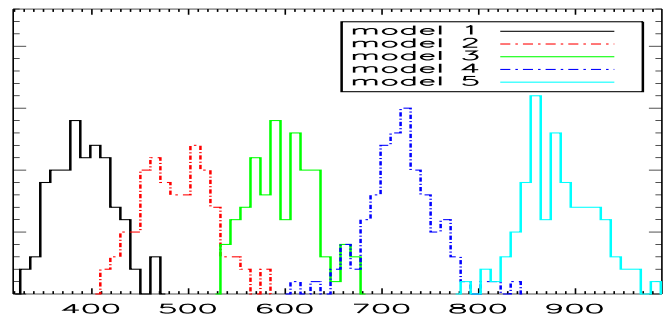


Figure 8. Distribution of the Wavelet Peak Counting estimated at the third scale of an Isotropic Wavelet Transform on the simulated realizations of the 5 models. It illustrates the results of the Table 7. We obtain a good discrimination even for adjacent models.

6. Discussion

As stated earlier, the formalism of the halo model provides a prediction for the number of clusters contained in a given field for a given cosmological model (Press and Schechter, 1974; Sheth and Tormen, 1999;

Ω_m is greatly improved using WPC estimated on MRLens filtered mass maps.

Hamana et al., 2004). However, we have to consider that just a fraction of the clusters, present in the sky, will be detected. It follows that we have to take into account the selection effects coming from the observation quality and the data processing method. The solution that is currently used consists in modeling the selection effects by estimating the selection function. An analytic model can be done by considering all the selection effects. An alternative consists in using a Monte Carlo approach that enables us to take into account the entirety of the selection effects that could not be considered in the analytic approach. This study will be done in a future work.

The selection function being specified, the connection with observations and theory is straightforward. The cosmological parameters can thus be estimated from *WPC*.

Having a perfect discrimination between the 5 cosmological models with *WPC* upper limits error on the cosmological parameters can be given by considering the spacing between two adjacent models. For space observations covering 4 square degrees, the upper limit error in σ_8 is 8%, in the range of $\sigma_8 \in [0.6, 1]$. And the upper limit error in Ω_m is 12%, in the range of $\Omega_m \in [0.23, 0.64]$. In future work, an accurate estimation of the error should be done.

7. Conclusion

Using only two-point statistics to constrain the cosmological model yield to various degeneracies between cosmological parameters such as the $(\sigma_8-\Omega_m)$ -degeneracy. In this paper, we survey a range of non-Gaussian statistics to set tighter constraints on cosmological parameters. For this purpose, we have run N-body simulations of 5 models selected along the $(\sigma_8-\Omega_m)$ -degeneracy and we have examined different non-Gaussian statistical tools in different representations in order to compare the discrimination power of each one. Using non-Gaussian statistics, we have looked for non-Gaussian signal present at small scales that is due to gravitational clustering.

The main conclusions of our analysis are the following:

1. The isotropic wavelet transform has been found to be the best representation of the non-Gaussian structures in weak lensing data allowing a better discrimination.
2. We have shown that a wavelet transform denoising method like the MRLens filtering, which reconstructs essentially the non-Gaussian structures (the clusters), helps the statistics to better characterize the non-Gaussianity.
3. We have introduced a new statistic called Wavelet Peak Counting (*WPC*) that consists in estimating a cluster count per scale of an isotropic wavelet transform.
4. *WPC* has been found to be the best statistic compared to the others that we have tested (skewness, kurtosis, bispectrum, HC, P_c) and we have shown that this statistic estimated on MRLens filtered maps provide a strong discrimination between the 5 selected models.

In this paper, we have compared systematically a wide range of non-Gaussian statistics proposed in the literature and *WPC* have been found to be the best statistic. The comparison being done on models selected along the $(\sigma_8-\Omega_m)$ -degeneracy, this study shows that the power spectrum (or the two-point correlation function) and *WPC* should therefore be used simultaneously. However, these two statistics probe the same field, therefore the correlations introduced by the combined measurement need to be taken into account (see Takada and Bridle, 2007). This will be investigated in the future.

Another issue, discussed in §6, is the selection effects. The selection function is needed for the estimation of the cosmological parameters and an accurate estimation of their errors. This study will be done in a future work.

Finally, while peak counting and *WPC* provide a lot of information, further statistics such as the cluster count per mass, the spatial cluster correlation will provide further constraints. Future work will be needed to fully exploit this approach.

Appendix A: The FDR method

False Discovery Rate (FDR) is a statistical approach to the multiple testing problem, introduced by Benjamini and Hochberg (1995).

The FDR method offers an effective way to select an adaptative threshold, without any assumption. The FDR threshold is determined from the observed p-value distribution, and hence is adaptive to the amount of signal in the data.

This technique has been described by Miller et al. (2001); Hopkins et al. (2002); Starck et al. (2006); Pires et al. (2006) with several examples of astrophysical applications. Instead of controlling the chance of any false positives, FDR controls the expected proportion of false positives. The FDR is given by the ratio

(12), that is, the proportion of declared active which are false positives:

$$\mathcal{FDR} = \frac{V_{ia}}{D_a} \quad (12)$$

where V_{ia} is the number of pixels truly inactive declared active, and D_a is the number of pixels declared active. The FDR formalism ensures that, *on average*, the False Discovery Rate is no larger than α which lies between 0 and 1. This procedure guarantees control over the FDR in the sense that:

$$\mathcal{E}(\mathcal{FDR}) \leq \frac{T_i}{V} \cdot \alpha \leq \alpha \quad (13)$$

The unknown factor $\frac{T_i}{V}$ is the proportion of truly inactive pixels where T_i is the number of inactive pixels and V the total number of pixels.

The FDR procedure is as follows :

Let P_1, \dots, P_n denote the p-values from the N tests, listed from smallest to largest.

Let :

$$d = \max\left\{k : P_k < \frac{k \cdot \alpha}{c_N \cdot N}\right\} \quad (14)$$

where $c_N = 1$, if p-values are statistically independent.

Now, declare activated all the pixels with p-values less than or equal to P_d .

Graphically, this procedure corresponds to plotting the P_k versus $\frac{k}{N}$, superposing the line through the origin of slope $\frac{\alpha}{c_N}$ (see Fig. 9), and finding the last point at which P_k falls below the line, termed P_d . From this p-value P_d , we can derive a threshold \mathcal{T} . All the pixels greater than \mathcal{T} have a p-value less than P_d and are declared actives.

Appendix B: The Higher Criticism definition

To define HC, first we convert the individual κ_i into p-values. Let $p_i = P\{N(0, 1) > \kappa_i\}$ be the i th p-value, and let $p_{(i)}$ denoted the p-values sorted in increasing order. The higher criticism statistic is defined as:

$$HC_n^* = \max_i \left| \frac{\sqrt{n}[i/n - p_{(i)}]}{\sqrt{p_{(i)}(1 - p_{(i)})}} \right|. \quad (15)$$

Or in a modified form :

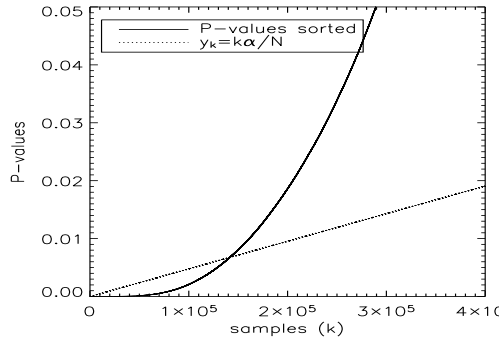


Figure 9. Finding a threshold graphically using the FDR procedure

$$HC_n^+ = \max_{i: 1/n \leq p_{(i)} \leq 1-1/n} \left| \frac{\sqrt{n}[i/n - p_{(i)}]}{\sqrt{p_{(i)}(1 - p_{(i)})}} \right|. \quad (16)$$

Appendix C: Description of the representations

The anisotropic bi-orthogonal wavelet transform

The most commonly used wavelet transform is the undecimated bi-orthogonal wavelet transform (OWT). Using the OWT, a 2D signal S can be decomposed as follows :

$$S(x, y) = \sum_{k_x, k_y} \phi_{J, k_x, k_y}(x, y) C_J(k_x, k_y) \quad (17)$$

$$+ \sum_d \sum_{k_x, k_y} \sum_{j=1}^J \psi_{J, k_x, k_y}^d(x, y) w_j^d(k_x, k_y), \quad (18)$$

with where ϕ and ψ^d are respectively the scaling function and the wavelet functions that prioritize the horizontal, vertical and diagonal directions. J is the number of resolutions used in the decomposition, w_j^d the wavelet (or detail) coefficients at scale j and direction d , and C_J is a smooth version of the original signal S .

The undecimated isotropic wavelet transform

The Undecimated Isotropic Wavelet Transform (UIWT) decomposes an $n \times n$ image κ as in :

$$\kappa(x, y) = C_J(x, y) + \sum_{j=1}^J w_j(x, y),$$

where C_J is a coarse or smooth version of the original image κ and w_j represents the details in κ at scale 2^j (see Starck and Murtagh, 2006, for details).

The ridgelet transform

The classical multiresolution ideas only address a portion of the whole range of interesting phenomena: the roughly isotropic one at all scales and all locations. The ridgelet transform have been proposed as an alternative to the wavelet representation of image data.

Given a function $f(x_1, x_2)$, the ridgelet transform is the superposition of elements of the form $a^{-1/2}\psi((x_1 \cos \theta + x_2 \sin \theta - b)/a)$, ψ is the wavelet, $a > 0$ the scale parameter, b the location parameter and θ the orientation parameter. The ridgelet is constant along lines $x_1 \cos \theta + x_2 \sin \theta = const$, and transverse to these ridges it is a wavelet.

The curvelet transform

Ridgelets are essentially focused on dealing with straight lines rather than curves, ridgelets can be adapted to representing objects with curved edges using an appropriate multiscale localization. If one uses a sufficiently fine scale to capture curved edges, such edges are almost straight. As a consequence the curvelet transform has been introduced, in which ridgelet are used in a localized manner.

The idea of the curvelet transform (Candès and Donoho, 1999; Starck et al., 2003) is to first decompose the image into a set of wavelet planes, then to decompose each plane in several blocks (the block size can change at each scale level) and to analyse each block with a ridgelet transform. The finest the scale is, the more sensitive to the curvature the analysis is. As a consequence, curved singularities can be well approximated with very few coefficients.

Appendix D: The MRLens filtering

The MRLens filtering (Starck et al., 2006) is a non linear filtering based on the Bayesian theory that searches for a solution that maximizes the a posteriori probability.

Choosing the prior is one of the most critical aspects of the Bayesian analysis. The MRLens filtering uses a multiscale entropy prior.

Assuming Gaussian noise, the MRLens filtering solves the following minimization :

$$J(\kappa) = \frac{\|\kappa_n - \kappa\|^2}{2\sigma_n^2} + \beta \sum_{j=1}^J \sum_{k,l} h_n((\mathcal{W}\kappa)_{j,k,l}) \quad (19)$$

where σ_n the noise standard deviation, J the number of scales, β is the regularization parameter and \mathcal{W} is the Wavelet Transform operator.

Full details of the minimization algorithm can be found in Starck et al. (2001), as well as the way to determine automatically the regularization parameter β .

In Starck et al. (2006), it has been shown that the MRLens filtering outperforms the existing methods. The MRLens filtering has already been used for several applications on weak lensing data and especially, it has been selected to filter the dark matter mass map obtained by the Hubble Space Telescope in the COSMOS field. The complete MRLens software package to perform weak lensing filtering can be downloaded from <http://www-irfu.cea.fr/Ast/878.html>.

References

- Aghanim, N. and Forni, O.: 1999, *A&A* **347**, 409
- Bacon, D. J., Massey, R. J., Refregier, A. R., and Ellis, R. S.: 2003, *MNRAS* **344**, 673
- Bahcall, N. A. and Fan, X.: 1998, *ApJ* **504**, 1
- Benabed, K. and Scoccimarro, R.: 2006, *A&A* **456**, 421
- Benjamin, J., Heymans, C., Semboloni, E., van Waerbeke, L., Hoekstra, H., Erben, T., Gladders, M. D., Hettterscheidt, M., Mellier, Y., and Yee, H. K. C.: 2007, *MNRAS* **381**, 702
- Benjamini, Y. and Hochberg, Y.: 1995, *J. R. Stat. Soc. B* **57**, 289
- Bernardeau, F., van Waerbeke, L., and Mellier, Y.: 1997, *A&A* **322**, 1
- Bernardeau, F., van Waerbeke, L., and Mellier, Y.: 2003, *A&A* **397**, 405
- Candès, E. and Donoho, D.: 1999, in A. Cohen, C. Rabut, and L. Schumaker (eds.), *Curve and Surface Fitting: Saint-Malo 1999*, Vanderbilt University Press, Nashville, TN

- Cooray, A. and Hu, W.: 2001, *ApJ* **548**, 7
- Dahle, H.: 2006, *Astrophysical Journal*
- Donoho, D. and Jin, J.: 2004, *Annals of Statistics* **32**, 962
- Fu, L., Semboloni, E., Hoekstra, H., Kilbinger, M., van Waerbeke, L., Tereno, I., Mellier, Y., Heymans, C., Coupon, J., Benabed, K., Benjamin, J., Bertin, E., Doré, O., Hudson, M. J., Ilbert, O., Maoli, R., Marmo, C., McCracken, H. J., and Ménard, B.: 2008, *A&A* **479**, 9
- Hamana, T., Takada, M., and Yoshida, N.: 2004, *MNRAS* **350**, 893
- Hoekstra, H., Mellier, Y., van Waerbeke, L., Semboloni, E., Fu, L., Hudson, M. J., Parker, L. C., Tereno, I., and Benabed, K.: 2006, *ApJ* **647**, 116
- Hoekstra, H., Yee, H. K. C., and Gladders, M. D.: 2002, *ApJ* **577**, 595
- Hopkins, A. M., Miller, C. J., Connolly, A. J., Genovese, C., Nichol, R. C., and Wasserman, L.: 2002, *Astronomical Journal* **123**, 1086
- Jarvis, M., Bernstein, G., and Jain, B.: 2004, *MNRAS* **352**, 338
- Jin, J., Starck, J.-L., Donoho, D. L., Aghanim, N., and Forni, O.: 2005, *EURASIP Journal on Applied Signal Processing, Vol. 2005, No 15, page 2470* **15**, 2470
- Kilbinger, M. and Schneider, P.: 2005, *A&A* **442**, 69
- Maoli, R., Van Waerbeke, L., Mellier, Y., Schneider, P., Jain, B., Bernardeau, F., Erben, T., and Fort, B.: 2001, *A&A* **368**, 766
- Massey, R., Refregier, A., Bacon, D. J., Ellis, R., and Brown, M. L.: 2005, *MNRAS* **359**, 1277
- Massey, R., Rhodes, J., Ellis, R., Scoville, N., Leauthaud, A., Finoguenov, A., Capak, P., Bacon, D., Aussel, H., Kneib, J.-P., Koekemoer, A., McCracken, H., Mobasher, B., Pires, S., Refregier, A., Sasaki, S., Starck, J.-L., Taniguchi, Y., Taylor, A., and Taylor, J.: 2007, *Nature* **445**, 286
- Massey, R., Rhodes, J., Refregier, A., Albert, J., Bacon, D., Bernstein, G., Ellis, R., Jain, B., McKay, T., Perlmutter, S., and Taylor, A.: 2004, *AJ* **127**, 3089
- Miller, C. J., Genovese, C., Nichol, R. C., Wasserman, L., Connolly, A., Reichart, D., Hopkins, A., Schneider, J., and Moore, A.: 2001, *Astronomical Journal* **122**, 3492
- Pen, U.-L., Lu, T., van Waerbeke, L., and Mellier, Y.: 2003, *MNRAS* **346**, 994
- Pires, S., Juin, J. B., Yvon, D., Moudren, Y., Anthoine, S., and Pierpaoli, E.: 2006, *AA* **455**, 741
- Pires, S., Starck, J., Amara, A., Teyssier, R., Fadili, J., and Refregier, A.: 2008, *submitted to MNRAS*
- Press, W. H. and Schechter, P.: 1974, *ApJ* **187**, 425
- Refregier, A., Rhodes, J., and Groth, E. J.: 2002, *APJL* **572**, L131
- Schneider, P.: 1996, *MNRAS* **283**, 837
- Schneider, P., Kilbinger, M., and Lombardi, M.: 2005, *A&A* **431**, 9
- Schneider, P. and Lombardi, M.: 2003, *A&A* **397**, 809
- Schneider, P., van Waerbeke, L., Jain, B., and Kruse, G.: 1998, *MNRAS* **296**, 873
- Semboloni, E., Mellier, Y., van Waerbeke, L., Hoekstra, H., Tereno, I., Benabed, K., Gwyn, S. D. J., Fu, L., Hudson, M. J., Maoli, R., and Parker, L. C.: 2006, *A&A* **452**, 51
- Sheth, R. K. and Tormen, G.: 1999, *MNRAS* **308**, 119
- Starck, J.-L., Abrial, P., Moudren, Y., and Nguyen, M.: 2006, *Astronomy and Astrophysics* **446**, 1191
- Starck, J.-L., Aghanim, N., and Forni, O.: 2004, *Astronomy and Astrophysics* **416**, 9
- Starck, J.-L., Aghanim, N., and Forni, O.: 2004, *A&A* **416**, 9
- Starck, J.-L., Candes, E., and Donoho, D.: 2003, *Astronomy and Astrophysics* **398**, 785
- Starck, J. L., Donoho, D. L., and Candès, E. J.: 2003, *A&A* **398**, 785
- Starck, J.-L. and Murtagh, F.: 2006, *Astronomical Image and Data Analysis*, Astronomical image and data analysis, by J.-L. Starck and F. Murtagh. Astronomy and astrophysics library. Berlin: Springer, 2006
- Starck, J.-L., Murtagh, F., Querre, P., and Bonnarel, F.: 2001, *Astronomy and Astrophysics* **368**, 730
- Starck, J.-L., Pires, S., and Réfrégier, A.: 2006, *A&A* **451**, 1139
- Takada, M. and Bridle, S.: 2007, *New Journal of Physics* **9**, 446
- Takada, M. and Jain, B.: 2003, *MNRAS* **344**, 857
- Takada, M. and Jain, B.: 2004, *MNRAS* **348**, 897
- Teyssier, R.: 2002, *A&A* **385**, 337
- Vale, C. and White, M.: 2003, *ApJ* **592**, 699
- Van Waerbeke, L., Mellier, Y., Pelló, R., Pen, U.-L., McCracken, H. J., and Jain, B.: 2002, *A&A* **393**, 369
- Vielva, P., Martínez-González, E., Barreiro, R. B., Sanz, J. L., and Cayón, L.: 2004, *Astrophysical Journal* **609**, 22
- Vielva, P., Wiaux, Y., Martínez-González, E., and Vanderghenst, P.: 2006, *New Astronomy Review* **50**,

880

Wiaux, Y., Vielva, P., Barreiro, R. B., Martínez-González, E., and Vandergheynst, P.: 2008, *MNRAS* **385**, 939